regions: the parent, the weld, the Heat Affected Zone (HAZ) and the Type IV materials as shown in Figure 8 [28]. The branch connection is subjected to a constant internal pressure of 4 (MPa) at 590°C. Hayhurst, Miller [28] have carried out a creep analysis of this branch geometry using two dimensional approximations to the Crotch and Flank sections shown in Figure 7a. The CDM methodology used is the outcome of research on high-temperature behaviour of welds carried out over two decades [29-37].

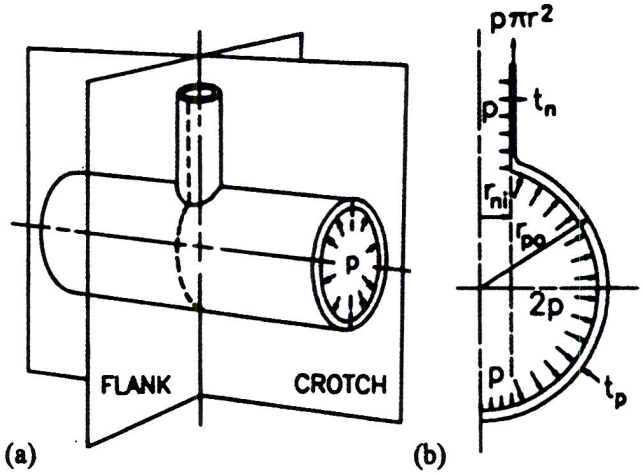

Figure 7. Definition of branch Crotch and Flank sections (a) and idealised sphere-cylinder equivalent applied pressure boundary conditions for Flank section (b); with r_{ni}=55.5, r_{po}=228, t_n=8, t_p=18, all dimensions are in mm.

The creep lifetime of the two sections have been determined by Hayhurst and Miller [28] using the CDM-based Finite Element solver DAMAGE XX. They have shown that the Flank section has a shorter lifetime. Hence, the analysis of the Flank section (see Figure 7b) is considered here.

Figure 7b shows that the Flank section is approximately modelled by application of twice the internal pressure, $2p$, on all internal surfaces except on the branch; and, by the application of the pressure p on its diametral projection. In this way, the model produces the actual in-plane stresses in the main pipe remote from the branch connection. However, the out-of-plane stresses in the main pipe are overestimated in the Flank model. Hence, this axi-symmetric model cannot model the real three-dimensional behaviour of the structure for two major reasons. Firstly, the assumed out-of-plane stress systems are different; and, secondly, the two Flank and Crotch sections (see Figure 7a) are assumed to be unconnected and therefore, they do not satisfy the compatibility of the nozzle end displacement. However, these differences are unlikely to have significant influence on the predicted damage initiation and growth modes. The results of a full three dimensional analysis are expected to show lower concentrations of stress but the damage initiation and growth patterns are likely to be unchanged.

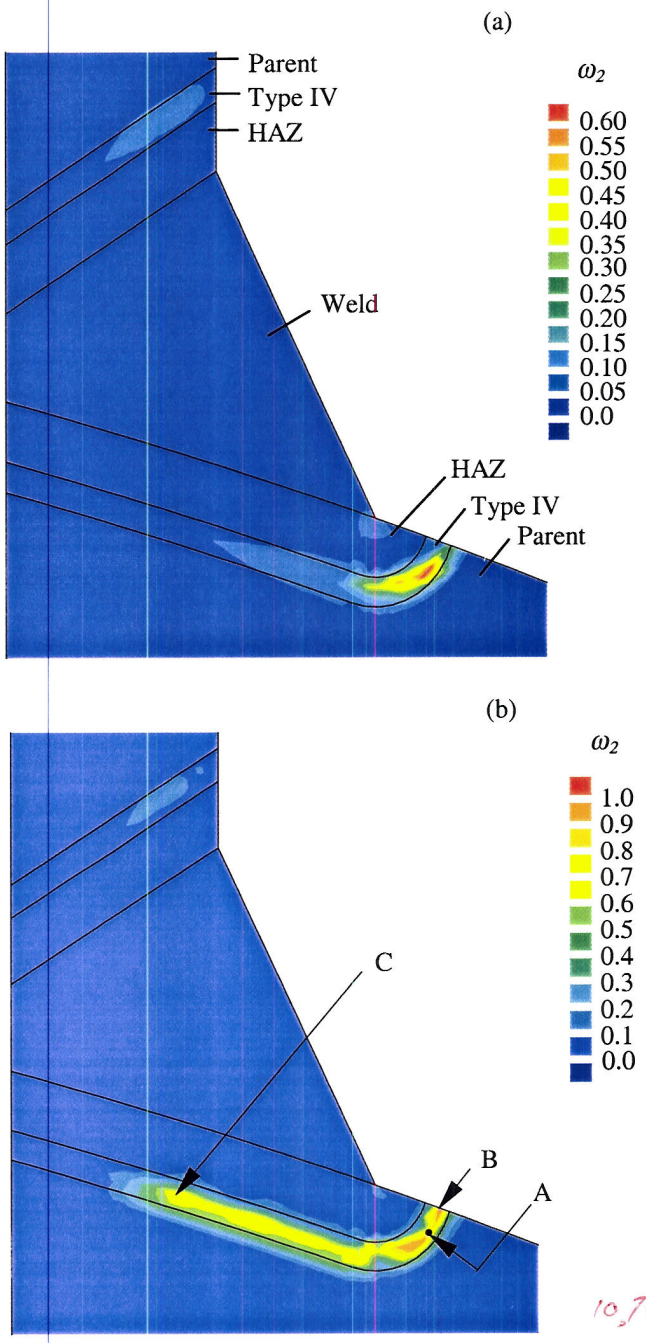

Figure 8. Damage fields, ω_2, for the axi-symmetric equivalent of the Flank section of the pressurised pipework branch connection after the initiation of the crack at 10 762 hours or t/t_f=0.763 (*a*) and when the inward crack (A-C) is 10 mm long at 13 845 hours or t/t_f=0.982 (*b*).

The Finite Element mesh used here to model the Flank section has 5 044 constant strain triangular elements and 5 584 degrees of freedom, with a global stiffness matrix half-bandwidth of 35; and, the smallest element is

0.03405 mm^2. The CDM analyses reported here have been carried out using DAMAGE XX with an enhanced time integration module due to Vakili-Tahami [38] which achieves greater accuracy and computational speed.

5.2 CDM-based Creep Crack Growth Predictions

Material behaviour. The creep behaviour of each of the distinct material regions is characterised using a set of hyperbolic-sine equations which are based on the underlying mechanisms of deformation and rupture pertinent to ferritic steels [28, 34, 35].

The model incorporates three state variables. The first state variable, H, is used to represent the strain hardening effect attributed to primary creep. Initially, H is zero and, as strain accumulates, it increases to a limiting value of H^*. The second state variable, Φ, describes the coarsening of the carbide precipitates, and is defined from the physics of ageing to vary from zero to unity. The coarsening of the carbide precipitates or ageing leads to a progressive loss in the creep resistance of particle hardened alloys such as ferritic steels. The third state variable, ω_2, represents inter-granular creep constrained cavitation damage and is chosen to vary from zero for the virgin state of metal to ω_{2f} at failure [39]. The multi-axial form of this set of constitutive equations is [28]:

$$\dot{\varepsilon}_{ij} = \frac{3 s_{ij}}{2 \sigma_e} A \sinh\left[\frac{B \sigma_e (1-H)}{(1-\Phi)(1-\omega_2)}\right], \qquad (8\,a)$$

$$\dot{H} = (h \dot{\varepsilon}_e / \sigma_e)\left[1 - \frac{H}{H^*}\right], \qquad (8\,b)$$

$$\dot{\Phi} = (k_c / 3)(1-\Phi)^4, \qquad (8\,c)$$

$$\dot{\omega}_2 = D N \dot{\varepsilon}_e (\sigma_1 / \sigma_e)^{\nu}. \qquad (8\,d)$$

The material parameters: A, B, D, h, H^* and k_c are constants to be determined from the uni-axial creep behaviour. The parameter ν is the multi-axial stress sensitivity index.

Hayhurst and Miller [28] using the methods due to Perrin and Hayhurst [34, 35] have determined the material parameters for constitutive Eq. (8) at the temperature of 590°C by extrapolation of the equations derived for 640°C by Perrin and Hayhurst [34, 35]. The value of the multi-axial stress rupture parameter ν and the failure criterion ω_{2f} are assumed to be those derived by Perrin and Hayhurst [35] for the same material at 640°C.

Due to the lack of any multi-axial creep rupture data for the material constituents of the weldment, the multi-axial rupture parameter, ν, has been assigned the same value as the parent material. This gives the same isochronous rupture loci for all constituents in bi-axial plane stress space.

DAMAGE XX predictions. Damage initiates 1-2 mm below the outer surface, at point A as shown in Figure 8b, in the Type IV region at the life fraction $t/t_f = 0.68$ and propagates in a very confined and crack like manner. The damage field is shown in Figure 8a after growth of a micro-crack ($t/t_f = 0.763$) in the Flank section. It can be seen that the damage growth is confined to the Type IV region close to the main pipe.

Figure 8b shows that the crack grows in both the outward (A-B) and the inward (A-C) directions. The crack first propagates in the outward direction and breaks through to the surface at point B; and, it then propagates rapidly in the inward direction towards C. Crack growth is modelled by removal of failed finite elements, and hence the crack length can be readily determined.

The propagation of the Type IV cracking predicted using the CDM-based model is presented in Figure 9. It can be seen that the crack propagation towards the pressurised surface (A-C) predominates with an increasing rate. The inward crack growth (A-C) rate increases significantly after the crack A-B breaks the surface. This would be expected since the crack then becomes an edge crack. It can be seen from Figure 9 that at the inward crack length of 10 mm measured along the A-C line (c.f. Figure 8b), the CDM-based crack growth rate is 12 mm/kh.

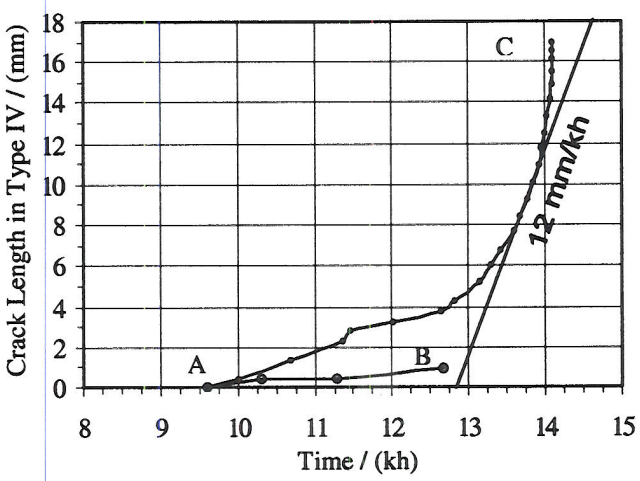

Figure 9. Type IV creep crack growth curves predicted using the CDM method for the axi-symmetric equivalent of the Flank section of the pressurised pipework branch connection. The crack length is measured along the outward (A-B) and the inward (A-C) growth directions. The inward crack growth rate is 12 mm/kh when the inward crack length (A-C) is 10 mm.

5.3 Estimates of Creep Crack Growth Using C^* Method Coupled with the R5 Code

For simplicity, crack growth rate calculations are confined to radial edge cracks (c.f. right hand sketch of Figure 1). In order to be comparable with DAMAGE XX predictions, the depth of an equivalent radial edge crack must be greater than that at which DAMAGE XX predicts break through to the outer surface. A radial edge crack

Need to state value of ω_{2f} (0.6?) in order for Fig. 8 to make sense to reader. Why > 0.6 in 8(b)?

depth of 8 mm from the main pipe side weld toe is considered, leaving a ligament of 6mm. Because of the curved portion of the crack in the CDM model (c.f. line A-C in Figure 8b) an 8 mm equivalent radial edge crack has been estimated as corresponding to 10 mm crack size measured along A-C in Figure 8b.

The assessment route R5 [5] predictions have been made using the results of the Finite Element code BERSAFE obtained by Qian [40] for the Flank geometry at 541°C, which is the plant design temperature. The value of C^* has been evaluated by Qian [40] for the vessel operating temperature of 541°C. However, for the purpose of this investigation C^* at 590°C is obtained using :

$$C^*(\text{at } 590°\text{C}) = \frac{\dot{\varepsilon}_{ref}\ (\text{at } 590°\text{C})}{\dot{\varepsilon}_{ref}\ (\text{at } 541°\text{C})}\, C^*\ (\text{at } 541°\text{C}). \qquad (9)$$

In the above equation, the reference creep strain rates, $\dot{\varepsilon}_{ref}$, are evaluated at the relevant reference stress, σ_{ref}, using the R5 code. The deformation data for the parent material used in the evaluation of the above creep strain rates at 590°C and 541°C at the time of interest $t=14\ 000$ [40] are:

Creep strain rate at 590°C = $4.4\text{x}10^{-5}$ (1/h)
Creep strain rate at 541°C = $2.0\text{x}10^{-7}$ (1/h)

The Finite Element analysis carried out by Qian [40] gives $C^*= 1.75\text{x}10^{-7}$ (MPa m/h) at 541°C when the equivalent radial edge crack length is 8 mm at $t=14\ 000$ hours. Substitution of the above values into Eq. (9) gives $C^*=3.9\text{x}10^{-5}$ (MPa m/h) at 590°C.

The creep crack growth rates, $\dot{a}$, are estimated using the following relationship:

$$\dot{a} = G(C^*)^q \qquad (10)$$

where G and q are constants given by the R5 code and are presented in Table 1.

Table 1. Material constants and parameters obtained using the R5 code for the Flank section with the estimated $C^*=3.9\text{x}10^{-5}$ (Mpa m/h) at 14 000 hour when the equivalent radial edge crack length is 8mm (corresponds to 10 mm crack size measured along A-C in Figure 8b).

Material	q	G (mm/h)	Creep crack Growth Rate, $\dot{a}$ (mm/kh)
Parent	0.80	60	18
Weld	0.67	14.6	16
HAZ	0.80	115	34
Type IV	0.76	18	8

From Table 1, it can be seen that the C^* method estimates the lowest creep crack growth rate of 8 (mm/kh) for the Type IV material, when the equivalent radial edge crack length is 8mm (see the right hand sketch of Figure 1).

5.4 Discussion and Implications

From Figure 9, it can be seen that the Type IV creep crack growth rate obtained using CDM model is 12 (mm/kh) for the crack length of 10 mm along the A-C line which is higher than that predicted by the R5 codes for the Type IV material, which is 8 (mm/kh); but, it is slower than the R5 rates predicted for the other materials (c.f. Table 1).

Table 2. Creep crack growth rate, $\dot{a}$, predicted using CDM-based model in the time range 13 280-14 080 hours.

Equivalent radial edge crack length (mm)	Crack A-C (mm)	Time (h)	$\dot{a}$ (mm/kh)
13.3	16	14 080	48
11.6	14	14 060	25
9.6	12	13 960	18
8	10	13 845	12
6	8	13 620	8
4	6	13 280	5.5

Examination of Table 2 shows that the CDM predictions of creep crack growth rate, $\dot{a}$, in the time range 13 280-14 080 changes from 5.5 to 48 (mm/kh) which highlights the difficulty of comparing values of $\dot{a}$ for a particular time. This range of $\dot{a}$ covers that given in Table 1 for all material phases of the weld.

It is worth noting that the crack growth behaviour in the Type IV zone is strongly constrained by both parent and HAZ materials, which in the CDM analyses are assumed to have the same properties. It might, therefore, be expected that the true C^* prediction be some combination of the values of $\dot{a}$ given in Table 1 for parent, HAZ and Type IV materials.

The CDM predictions of 12 (mm/kh) compare well with the C^* predictions $\dot{a}$ given in Table 1 over the time range 13 280-14 080 hours.

6. CONCLUSIONS

CDM has been shown to be capable of predicting the behaviour of a range of structures from simple plane stress concentrations, to notched bars, to creep crack growth in plane strain cracked members and to compact tension specimens (CTS).